

Practical selection of emission lines of He I to determine the photon absorption rate

Cite as: Rev. Sci. Instrum. **82**, 023501 (2011); <https://doi.org/10.1063/1.3548923>

Submitted: 13 September 2010 . Accepted: 06 January 2011 . Published Online: 10 February 2011

Shin Kajita, and Noriyasu Ohno



View Online



Export Citation

ARTICLES YOU MAY BE INTERESTED IN

[Comparison of He I line intensity ratio method and electrostatic probe for electron density and temperature measurements in NAGDIS-II](#)

Physics of Plasmas **13**, 013301 (2006); <https://doi.org/10.1063/1.2164461>

[Optical diagnostics with radiation trapping effect in low density and low temperature helium plasma](#)

Physics of Plasmas **23**, 063516 (2016); <https://doi.org/10.1063/1.4954047>

[Helium I line intensity ratios in a plasma for the diagnostics of fusion edge plasmas](#)

Review of Scientific Instruments **67**, 3521 (1996); <https://doi.org/10.1063/1.1147060>



Practical selection of emission lines of He I to determine the photon absorption rate

Shin Kajita¹ and Noriyasu Ohno²

¹*EcoTopia Science Institute, Nagoya University, Nagoya 464-8603, Japan*

²*Graduate School of Engineering, Nagoya University, Nagoya 464-8603, Japan*

(Received 13 September 2010; accepted 6 January 2011; published online 10 February 2011)

A combination of helium line intensities and a collisional radiative model has been used to measure electron density and temperature. However, radiation trapping of resonance lines may disturb the measurements due to disturbances in the population distribution of helium atoms. In this study, we show that the principal contribution of radiation trapping in helium plasma can be evaluated by additionally measuring one or two specific line intensities from the singlet state. The inclusion of the effects of radiation trapping sufficiently compensates for anomalous increases in the electron density and temperature, and consequently yields proper values. An experiment was performed in the divertor simulator NAGDIS-II, and the method's validity was confirmed by comparing the spectroscopically obtained results and the values from the electrostatic probe method. © 2011 American Institute of Physics. [doi:10.1063/1.3548923]

I. INTRODUCTION

Measurement of electron density n_e and temperature T_e in the divertor region of fusion devices is important for controlling the edge plasma and sustaining the overall plasma performance. A helium line intensity method has been used to measure n_e and T_e in many fusion devices including TEXTOR (Tokamak Experiment for Technology Oriented Research),¹ JET (Joint European Torus),² JT-60U (Japan Torus-60 Upgrade),³ and LHD,⁴ and linear devices, Nagoya Divertor Simulator-I (NAGDIS-I),⁵ MAP (Material and Plasmas)-II,⁶ NAGDIS-II,⁷ and PISCES-A.⁸ This method's advantage is its simplicity; it uses only a few line emission intensities from helium neutrals that should be produced by nuclear reactions. Radiation trapping of vacuum ultraviolet resonance lines significantly alters the intensity ratios^{5,6} and leads to overestimation of n_e and T_e .⁷ An optical escape factor and a ray tracing simulation have been successfully used to understand and estimate the radiation trapping effects in divertor simulators.⁵⁻⁹ However, the optical escape factor method can be applied to only simple configurations, such as cylindrical and planar configurations. It also requires several parameters, such as the neutral temperature and radiation trapping radius that has been regarded as radius of cylinder,¹⁰ but the estimation of the radius is a difficult issue. Moreover, the conventional optical escape factor method can be applied only to the center of a plasma column and not to the peripheral region.⁷ A formula for radiation trapping considering the spatial profile of plasma was recently reported.^{11,12} Although it has been successfully applied to the peripheral region, the method also requires spatial density profiles of the upper state. A ray tracing simulation is a good method for understanding the effects of radiation trapping in detail;⁹ however, it seems difficult to apply it as a measurement method.

Recently, Sawada *et al.* directly estimated the photon absorption rates by measuring 16 helium line intensities.¹³ Although direct estimation of the photon excitation rate can yield proper T_e and n_e , it is difficult in practice to measure

so many line intensities simultaneously at a good time resolution. In this paper, for practicality, a much simpler method is developed considering the radiation trapping effect; it is shown that only one or two line intensities are required to be added to a conventional line intensity method to estimate the principal contribution of the photon excitation rate and proper n_e and T_e . This simple method does not require complicated parameters, such as the radiation trapping radius and neutral temperature. Moreover, it can also be applied to a peripheral region of the plasma column, where the conventional optical escape factor method for the center of the plasma¹⁰ cannot be applied. In this paper, the principle of the method is described in Sec. II; in Sec. III, to verify the method, the spectroscopic and electrostatic probe methods are compared using the divertor simulator NAGDIS-II (Nagoya Divertor Simulator).

II. METHOD

Population distribution of helium atoms is calculated using a He I collisional-radiative model code, the so-called Goto code.⁴ In addition to the conventional collisional-radiative code, a photon absorption rate representing the atomic density excited by the reabsorption process per unit time is introduced to the n^1P states, where n is the principal quantum number. In other words, for n^1P states, the photon absorption rate, $K(n^1P)$ ($\text{m}^{-3}\text{s}^{-1}$), is added to the rate equation shown below. The temporal evolution of the excited state population $n(p)$ of a level p is written as

$$\begin{aligned} \frac{dn(p)}{dt} = & - \left[\sum_{q \neq p} C(p, q)n_e + \sum_{q < p} A(p, q) + S(p)n_e \right] n(p) \\ & + \sum_{q \neq p} [C(q, p)n_e + A(q, p)]n(q) \\ & + [\alpha(p)n_e + \beta(p) + \beta_d(p)]n_i n_e \\ & + \delta_{p,2^1P} K(2^1P) + \delta_{p,3^1P} K(3^1P) \\ & + \delta_{p,4^1P} K(4^1P) + \dots, \end{aligned} \quad (1)$$

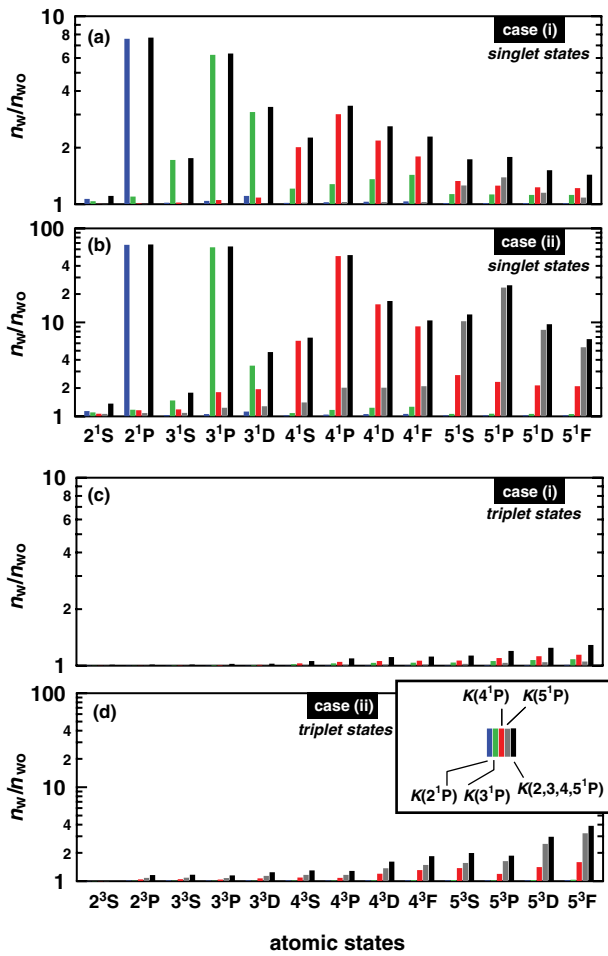


FIG. 1. (Color online) Calculated densities of (a) single and (b) triplet states normalized to the ones without radiation trapping effect. For each state, five calculated results are shown. From left, $K(2^1P)$, $K(3^1P)$, $K(4^1P)$, and $K(5^1P)$ are considered, respectively, and all the effects are included in the most right one..

where $A(p, q)$ is the spontaneous transition probability from p to q , $C(p, q)$ and $S(p)$ are the rate coefficients for electron impact transition (excitation or de-excitation) and ionization, respectively; $\alpha(p)$, $\beta(p)$, and $\beta_d(p)$ are the rate coefficients for three-body, radiative, and dielectronic recombination, respectively; n_i is the singly ionized helium density; and $\delta_{p,2^1P}$, $\delta_{p,3^1P}$, and $\delta_{p,4^1P}$ mean Kronecker delta that are one if the two states denoted by the subscript are the same and zero otherwise. The equation is coupled with the equations for other states, and consequently, the population density $n(p)$ can be deduced. Note that quasisteady-state approximation is applied for all states except the ground state because the lifetimes of metastable states are much shorter than the characteristic time for the transport of helium atoms under the present conditions.⁷

Without radiation trapping, the free parameters required to solve the series of Eq. (1) are n_e , T_e , and the neutral density assuming $n_i = n_e$. When photon absorption effects are considered, $K(n^1P)$ also becomes free parameter. In Ref. 9, the photon absorption rates were determined by conducting a ray tracing simulation. From a practical point of view, in the present study, $K(n^1P)$ is introduced in Eq. (1) and

determined by measuring the other line intensities which are sensitive to $K(n^1P)$. The method is basically the same as in Ref. 13, although the selected lines used for optimization differ. With regard to optimization point of view, it is important to consider the absorption rates that we introduce. If rates that do not have significant sensitivity to the measured lines are introduced, the calculation would produce physically meaningless values. In general, the values would be significantly larger by many orders of magnitudes than the expected ones, negatively affecting the evaluation of other parameters. Thus, we next discuss the sensitivity of the absorption rates to the population distribution, because they are important when introducing $K(n^1P)$ and choosing the lines to be measured.

Figures 1(a)–1(d) show the calculated population densities normalized by those without radiation trapping effects in two different cases, case (i) and (ii). Figures 1(a) and 1(b) correspond to singlet states, and Figs. 1(c) and 1(d) correspond to triplet states. Also, Figs. 1(a) and 1(c) correspond to case (i), whereas Figs. 1(b) and 1(d) correspond to case (ii). The neutral density is assumed to be 2 mTorr, and the electron density and temperature are assumed to be 10^{19} m^{-3} and 5 eV, respectively, in case (i), and 10^{18} m^{-3} and 2 eV, respectively, in case (ii). To discuss the contribution from each absorption rate separately, five calculations are made: cases in which each of the four rates $K(2^1P)$, $K(3^1P)$, $K(4^1P)$, and $K(5^1P)$ is considered, and a case in which all of them are together taken into consideration. Here, n_{w0} is defined as the density without any absorption rates, and $n_{w:n}$ is the density after the introduction of the absorption rate $K(n^1P)$. In Fig. 1, $n_{w:2}/n_{w0}$, $n_{w:3}/n_{w0}$, $n_{w:4}/n_{w0}$, $n_{w:5}/n_{w0}$, and $n_{w:2-5}/n_{w0}$ are shown as different-colored bars. In this case study, the absorption rate was assumed to be the same as the emission rate without radiation trapping, namely $n_{w0}(n^1P)A_{n^1P,1^1S}$. This simulates a realistic situation. In fact, in a previous experiment, the density in the 3^1P state was more enhanced than those in this case study at the peripheral region.⁹

Figure 1 shows that the triplet states do not change much with the radiation trapping, although the singlet states are significantly altered by its effects. The enhancement rate is large for n^1P states, and the enhancement affects the population densities in the singlet states with the same n . For example, focusing on $n_{w:3}/n_{w0}$, the densities in 3^1S , 3^1P , and 3^1D are increased, but the other states with higher or lower n are not altered much. In the same manner, focusing on $n_{w:4}/n_{w0}$, significant increase occurs in the densities in 4^1S , 4^1P , 4^1D , and 4^1F . However, $n_{w:4}(3^1P)/n_{w0}$ is approximately two in Fig. 1(b), indicating that it contributes to the enhancement of $n_{w:2-5}(3^1P)/n_{w0}$ by several tens of percent. The case study indicates that principal contributions of the radiation trapping effects can be estimated by introducing the absorption rate with the same n . In addition, to estimate the enhancement rate more accurately, it is better to introduce the absorption rate with the principal quantum number $n + 1$. Under some conditions, the influence of $K(2^1P)$ on $n = 3$ states might not be negligible, although it should be minor, as was discussed in Ref. 11. There might be a practical way to determine $K(2^1P)$ with certain assumptions without using vacuum ultraviolet measurements. However, in this study, we neglected the influence of $K(2^1P)$ on the basis of the discussion in this section,

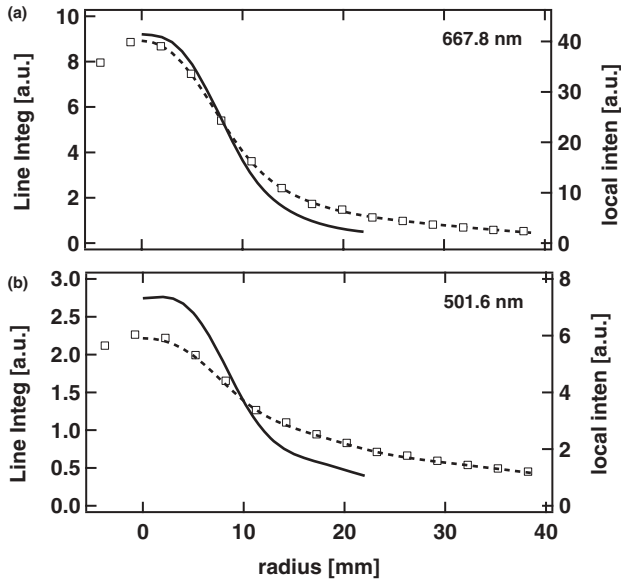


FIG. 2. (a) and (b) show the emission profiles of the $2^1\text{P}-3^1\text{D}$ (667.8 nm) and $2^1\text{S}-3^1\text{P}$ (501.6 nm) transitions, respectively. The dotted lines are fitting curves for the experimental values represented as symbols. The solid curves are the local intensities deduced from the Abel inversion method.

because the effect seemed to be minor compared to the singlet 3P, 4P, and 5P states.

One set of proposed line intensities for the measurement of n_e and T_e is the lines at 667.8 ($2^1\text{P}-3^1\text{D}$), 706.5 ($2^3\text{P}-3^3\text{S}$), and 728.1 nm ($2^1\text{P}-3^1\text{S}$). Because the principal quantum number of all the upper states of the emission is three, the dominant contribution of the radiation trapping can be included by estimating $K(3^1\text{P})$. The case study suggests that it may be better if $K(4^1\text{P})$ is also added. To estimate $K(3^1\text{P})$, we can choose the $2^1\text{S}-3^1\text{P}$ transition at 501.6 nm. As for $K(4^1\text{P})$, there are three candidate lines: the $2^1\text{P}-4^1\text{S}$ transition at 504.8 nm, the $2^1\text{S}-4^1\text{P}$ transition at 396.5 nm, and the $2^1\text{P}-4^1\text{D}$ transition at 492.2 nm. The line at 492.2 nm had the largest intensity and its wavelength was close to that of the $2^1\text{P}-4^1\text{S}$ transition; we chose it as a sensitive line for $K(4^1\text{P})$, regarding as the best one in practical terms.

III. EXPERIMENTAL VERIFICATION

To validate the method, an experiment was performed in the divertor simulator NAGDIS-II. Details of the experimental setup are given in Ref. 7. Using arc discharge a 2 m helium plasma was produced whose shape was columnar owing to the magnetic field formed with solenoidal coils, and the magnetic field strength was 0.1 T. The line intensities were measured using a Czerny–Turner spectrometer. The local intensities were deduced from the line-integrated emission profile by using an Abel inversion method.⁷ To reduce the numerical error in the Abel inversion process, we used the following even function to fit the measured line integrated emission profiles:

$$I(r) = (B_0 + B_1r^2 + B_2r^4 + B_3r^6) \exp(-A_0r^2) + B_4r^2 \exp(-A_1|r|), \quad (2)$$

where A_0 , A_1 , and $B_0 - B_4$ are the fitting parameters. Figures 2(a) and 2(b) show the emission profiles for the $2^1\text{P}-3^1\text{D}$ (667.8 nm) and $2^1\text{S}-3^1\text{P}$ (501.6 nm) transitions, respectively. The dotted lines are the fitting curves for the experimental values, which are represented by symbols. The emission profile at 501.6 nm is significantly broader than that at 667.8 nm. From a previous investigation,⁹ this broadening can be attributed to radiation transport. Although the emission profiles at 706.5 nm, and 728.1 nm are not shown here, they are unbroadened similar to that at 667.8 nm. The solid curves are the local intensities deduced from the Abel inversion method. In the method, the value at $r = r_0$ is obtained from the intensity profile at the outside from the point, that is, at $r > r_0$; in particular, the edge profile is very important. Because the measurement was performed at $r < 40$ mm, ambiguity remains regarding the edge of the emission at 501.6 nm, especially because the profile is significantly broadened. Not to reflect this numerical error, only the local values at $r \leq 20$ mm are used in later calculations. Moreover, the fitted function was extrapolated to $r \sim 60$ mm to reduce numerical errors.

To obtain n_e and T_e from the measured line intensities, it is necessary to minimize the error between the experiments and calculations with changing n_e , T_e , and absorption rates. When there are two free parameters, optimization is rather easy; however, it becomes difficult as the number of free parameters increases. Here, we use a simulated annealing method,¹⁴ which is a generic probabilistic algorithm for global optimization. In particular, the so-called Metropolis algorithm is used for the annealing process.¹⁵ The simulated annealing method becomes a powerful tool, particularly when the number of free parameters is large. Here, we briefly describe the optimization process. When radiation trapping is not considered, two line intensity ratios, $I(667.8)/I(728.1)$ and $I(728.1)/I(706.5)$, are used for optimization. The line intensity ratio $I(501.6)/I(728.1)$ is introduced to estimate $K(3^1\text{P})$; and moreover, the intensity ratio of $I(492.2)/I(728.1)$ is introduced for $K(4^1\text{P})$, additionally. The line intensity ratios $I(667.8)/I(728.1)$, $I(728.1)/I(706.5)$, $I(501.6)/I(728.1)$, and $I(492.2)/I(728.1)$ are written as κ_1 , κ_2 , κ_3 , and κ_4 , respectively. Experimental and numerical values are distinguished by superscripts κ^{exp} and κ^{cal} , respectively. The best set of free parameters is chosen to minimize the evaluation function

$$\text{error} = \sqrt{\sum_{i=1}^N \left(\frac{\kappa_i^{\text{exp}} - \kappa_i^{\text{cal}}}{\kappa_i^{\text{exp}}} \right)^2}, \quad (3)$$

where N is the number of optimized parameters. When $N = 2$, the effect of radiation trapping is not included, and the free parameters are n_e and T_e . When $N = 3$, the free parameter $K(3^1\text{P})$ is introduced, and when $N = 4$, the free parameter $K(4^1\text{P})$ is introduced.

First, we assume that the absorption rates are zero and calculate the error from Eq. (3). The calculated error is called E_{opt} . In the next calculation, the free parameters are changed using a Monte Carlo method that includes the absorption rates. When the newly calculated error E_{tmp} is smaller than E_{opt} , the state, i.e., the set of optimized values here, is

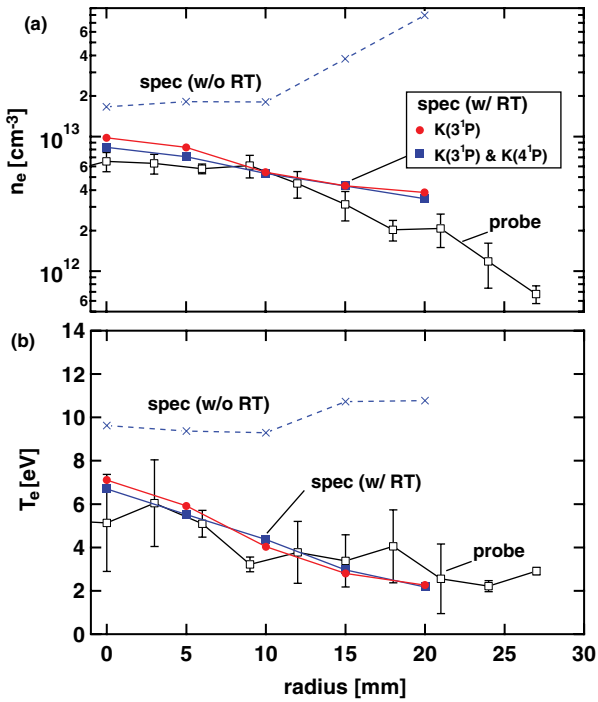


FIG. 3. (Color online) Comparisons of (a) electron density and (b) electron temperature between the electrostatic probe and line intensity methods for $N = 2, 3$, and 4 .

changed promptly with a probability of 100%. Even when E_{tmp} is larger than E_{opt} , the state can be changed with the probability

$$p = \exp\left(-\frac{E_{\text{tmp}} - E_{\text{opt}}}{T_{SA}}\right), \quad (4)$$

where T_{SA} is the control parameter. The Monte Carlo method is used to determine whether to change the state. If the state is changed, the provisionally optimized state is changed to the newly calculated state, and E_{opt} is replaced by the new value E_{tmp} . Repetitive calculations of E_{tmp} and comparisons with E_{opt} are done by changing the free parameters. During the calculation, T_{SA} gradually decreases. Therefore, because the rates of variation in the free parameters, i.e., $\Delta T_e/T_e$, $\Delta n_e/n_e$ and $\Delta K(n^1P)/K(n^1P)$ are related to T_{SA} in our code, the variation in the free parameters also decreases. The optimization is completed after a sufficient number of calculations.

The results of the electrostatic probe and spectroscopic methods are compared in Figs. 3(a) and 3(b) for n_e and T_e , respectively. The density and temperature at $r \sim 0$ mm are approximately $6 \times 10^{18} \text{ m}^{-3}$ and 6 eV, respectively, from the electrostatic probe, and both the values decrease with r . For the spectroscopic method, both the density and temperature anomalously increase with r when $N = 2$ in which case radiation trapping is not taken into account. Moreover, both values are considerably higher in the spectroscopic method than those in the electrostatic probe. On the other hand, when $N = 3$ and 4 , both n_e and T_e are lower than those at $N = 2$ and approach the values from the electrostatic probe. Furthermore, they decrease with r , and agreeing well with those from the probe. Note that no significant difference appeared between $N = 3$ and 4 in this study. The results confirm that the measurement of additional line intensities compensates

for the principal contribution of radiation trapping and yields appropriate values of n_e and T_e .

In the divertor region of fusion devices, n_e is comparable to or higher than that in the present study, and the helium neutral density may be lower because the fraction of helium is maximum 10%. On the basis of these facts and the investigation carried out in this study, it is thought that the introduction of additional line intensity at 501.6 nm can sufficiently compensate for the error caused by radiation trapping even in the divertor region. This additional line intensity will broaden the applicability of the helium line intensity method.

IV. CONCLUSION

In summary, a modified line intensity method including the effect of radiation trapping has been developed and its validity has been confirmed experimentally. A case study calculation revealed that an enhancement of the n^1P state due to radiation trapping, where n is the principal quantum number, affects primarily the population density of singlet states with the same n . Moreover, it was found that the enhancement of the 2^1P state due to the radiation trapping of 1^1S-2^1P transition does not have considerable influences to the population density with higher n , in agreement with the recent report of Sawada *et al.*¹³ The principal contribution of radiation trapping to the proposed line intensity method by using the line intensities at 667.8, 706.5, and 728.1 nm has been estimated by measuring the line from the 3^1P state and a singlet state with $n = 4$. Previously, the emission intensity of the 2^1S-3^1P transition had been used to estimate the radiation trapping radius,¹⁶ which is important for estimating the optical escape factor. On the other hand, in the method of this study, the radiation trapping effect can be directly considered by estimating the photon absorption rate from the emission intensity of the 2^1S-3^1P transition. The advantage of this method is that the effect of radiation trapping can be taken into account without considering the neutral temperature and neutral density profiles, which are necessary for estimating the optical escape factor. This method can also be used in the peripheral region of the plasma column, where a conventional optical escape factor method cannot be applied. Although the line intensity method without radiation trapping yielded considerably higher n_e and T_e than those yielded using the electrostatic probe, it successfully produced values in agreement with those using the electrostatic probe after radiation trapping was considered by measuring one or two additional line intensities. This method can be a practical technique for measuring n_e and T_e in the divertor region of fusion devices even when the effect of radiation trapping cannot be neglected.

ACKNOWLEDGMENTS

The authors thank Dr. M. Goto at National Institute for Fusion Science for providing us with his excellent collisional-radiative code. Fruitful discussions with Mr. Y. Iida at the University of Tokyo are appreciated. This work is supported by a Grant-in-Aid for Young Scientists (B) 21760690 and a

Grant-in-Aid for Scientific Research (A) 22246120 from Japan Society for the Promotion of Science.

- ¹B. Schweer, G. Mank, A. Pospieszczyk, B. Brosda, and B. Pohlmeier, *J. Nucl. Mater.* **196–198**, 174 (1992).
- ²S. J. Davies, P. D. Morgan, Y. Ul’Haq, C. F. Maggi, S. K. Ereents, W. Fundamenski, L. D. Horton, A. Loarte, G. F. Matthews, R. D. Monk, and P. C. Stangeby, *J. Nucl. Mater.* **241–243**, 426 (1997).
- ³H. Kubo, M. Goto, H. Takenaga, A. Kumagai, T. S. S. Sakurai, N. Asakura, S. Higashijima, and A. Sakasai, *J. Plasma Fusion Res.* **75**, 945 (1999).
- ⁴M. Goto, *J. Quant. Spectrosc. Radiat. Transf.* **76**, 331 (2003).
- ⁵S. Sasaki, S. Takamura, S. Watanabe, S. Masuzaki, T. Kato, and K. Kadota, *Rev. Sci. Instrum.* **67**, 3521 (1996).
- ⁶Y. Iida, S. Kado, A. Okamoto, S. Kajita, T. Shikama, D. Yamasaki, and S. Tanaka, *J. Plasma Fusion Res. Series 7*, 123 (2006).
- ⁷S. Kajita, N. Ohno, S. Takamura, and T. Nakano, *Phys. Plasmas* **13**, 013301 (2006).
- ⁸D. Nishijima and E. M. Hollmann, *Plasma Phys. Controlled Fusion* **49**, 791 (2007).
- ⁹S. Kajita, D. Nishijima, E. M. Hollmann, and N. Ohno, *Phys. Plasmas* **16**, 063303 (2009).
- ¹⁰T. Fujimoto, *Plasma spectroscopy* (Clarendon, Oxford, 2004).
- ¹¹Y. Iida, S. Kado, A. Muraki, and S. Tanaka, *Rev. Sci. Instrum.* **81**, 10E511 (2010).
- ¹²Y. Iida, S. Kado, and S. Tanaka, *Phys. Plasmas* **17**, 123301 (2010).
- ¹³K. Sawada, Y. Yamada, T. Miyachika, N. Ezumi, A. Iwamae, and M. Goto, *J. Plasma Fusion Res.* **5**, 001 (2010).
- ¹⁴W. H. Press, S. A. Teukolsky, W. T. Vetterling, and B. P. Flannery, *Numerical Recipes in C 1st ed.* (Cambridge University Press, 1988).
- ¹⁵N. Metropolis, A. W. Rosenbluth, M. N. Rosenbluth, and A. H. Teller, *J. Chem. Phys.* **21**, 1087 (1953).
- ¹⁶F. Scotti and S. Kado, *J. Nucl. Mater.* **390–391**, 303 (2009).